Laser Controlled Spin Dynamics of Ferromagnetic Thin Film from Femtosecond to Nanosecond Timescale

Sucheta Mondal and Anjan Barman*

Department of Condensed Matter Physics and Material Sciences, S. N. Bose National Centre for Basic Sciences, Block JD, Sector III, Salt Lake, Kolkata 700 106, India

Laser-induced modulation of the magnetization dynamics occurring over various timescales are unified here for a $Ni_{80}Fe_{20}$ thin film excited by amplified femtosecond laser pulses. The weak correlation between demagnetization time and pump fluence with substantial enhancement in remagnetization time is demonstrated using a three-temperature model considering the temperatures of electron, spin, and lattice. The picosecond magnetization dynamics is modeled using the Landau-Lifshitz-Gilbert equation. With increasing pump fluence the Gilbert damping parameter shows significant enhancement from its intrinsic value due to an increment in the ratio of electronic temperature to Curie temperature within a very short timescale. The precessional frequency experiences a noticeable redshift with increasing pump fluence. The changes in the local magnetic properties due to accumulation and dissipation of thermal energy within the probed volume are described by the evolution of the temporal chirp parameter in a comprehensive manner. A unification of ultrafast magnetic processes and its control over a broad timescale will enable the integration of various magnetic processes in a single device and use one effect to control another.

I. INTRODUCTION

Recent developments in magnetic storage [1] and memory [2] devices heavily rely on increasing switching speed and coherent switching of magnetic states in ferromagnetic thin films and patterned structures. Operating speeds of information storage devices have progressed into the subgigahertz regime and controlled switching in individual layers of magnetic multilayers and heterostructures has become important. The relaxation processes involved in magnetization dynamics set natural limits for these switching times and data transfer rates. In the context of precessional magnetization dynamics, the natural relaxation rate against a small perturbation is expressed as Gilbert damping (α) according to the Landau-Lifshiz-Gilbert (LLG) equation [3,4]. This is analogous to the viscous damping of mechanical-frictional torque and leads to the direct dissipation of energy from the uniform precessional mode to a thermal bath in the case of zero wavevector excitation. Gilbert damping originates from spin-orbit coupling and depends on the coupling strength and d band width of the $3d$ ferromagnet [5]. The damping can be varied by various intrinsic and extrinsic mechanisms including phonon drag [6], eddy current [7], doping [8] or capping [9] with another material, injection of spin current [10], magnon-magnon scattering [11], and controlling the temperature of the system [12]. The intrinsic and

extrinsic natures of Gilbert damping are primarily studied by using ferromagnetic resonance (FMR) technique. When the magnetization is aligned with either the in-plane or out-of-plane applied magnetic field, the linewidth is proportional to the frequency with a slope determined by the damping coefficient. This is the homogeneous or intrinsic contribution to the FMR linewidth. However, experiments show an additional frequency-independent contribution to the linewidth that corresponds to inhomogeneous line broadening [13,14]. A state-of-the-art technique based on pump-probe geometry has been developed and rigorously exploited for measuring the ultrafast magnetization dynamics of ferromagnetic thin films during the last few decades [15,16]. Using the time-resolved magneto-optical Kerr effect (TR MOKE) technique, one can directly address the processes which are responsible for the excitation and relaxation of a magnetic system on their characteristic timescales [17–19]. Generally, during the pump-probe measurements, pump fluence is kept low to avoid nonlinear effects and sample surface degradation. Some recent experiments reveal that nonlinear spin waves play a crucial role in high-power thin-film precessional dynamics by introducing spin-wave instability [20] similar to FMR experiments by the application of a high-rf power [21]. The coercivity and anisotropy of the ferromagnetic thin films can also be lowered by pump fluence, which may have potential applications in heat-assisted magnetic recording (HAMR) [22]. Recent reports reveal that the damping coefficient can be increased or decreased

----

*abarman@bose.res.in

noticeably in the higher excitation regime due to the opening of further energy dissipation channels beyond a threshold pump power [23–25]. Not only relaxation parameters, but also a frequency shift due to enhancement in the pump power has been observed [20]. However, experimental evidence for a large modulation of Gilbert damping along with the frequency shift and temporal chirping of the uniform precessional motion is absent in the literature. This investigation requires a suitable choice material be chosen, and here we have chosen Permalloy ($Ni_{80}Fe_{20}$ or Py hereafter) because of its high permeability, negligible magneto-crystalline anisotropy, very low coercivity, and large anisotropic magnetoresistance with reasonably low damping. Also, due to its negligible magnetostriction, Py is less sensitive to strain and stress exerted during the thermal treatment in HAMR [22].

In this article, we use femtosecond amplified laser pulses for excitation and detection of ultrafast magnetization dynamics in a Py thin film. Pump fluence-dependent ultrafast demagnetization is investigated along with fast and slow remagnetization. Our comprehensive study of the picosecond dynamics reveals the transient nature of enhanced Gilbert damping in the presence of high pump fluence. Also, the time-varying precession is subject to temporal chirping, which occurs due to enhancement of the temperature of the probed volume within a very short timescale followed by successive heat dissipation. This fluence-dependent modulation of magnetization dynamics will undoubtedly find suitable applications in spintronic and magnonic devices.

II. SAMPLE PREPARATION AND CHARACTERIZATION

20-nm-thick Py film is deposited using an electron-beam evaporation technique (SVT Associates, model: Smart Nano Tool AVD-E01) (base pressure $= 3 \times 10^{-8}$ Torr, deposition rate $= 0.2$ Å/S) on an 8×8 mm^2 silicon (001) wafer coated with 300-nm-thick SiO_2. Subsequently, 5-nm-thick SiO_2 is deposited over the Py using a rf sputter-deposition technique (base pressure $= 4.5 \times 10^{-7}$ Torr, Ar pressure $= 0.5$ mTorr, deposition rate $= 0.2$ Å/S, rf power $= 60$ W). This capping layer protects the surface from environmental degradation, oxidation, and laser ablation during the pump-probe experiment using femtosecond laser pulses. From the vibrating sample magnetometry (VSM) we have determined the saturation magnetization (M_s) and Curie temperature (T_c) to be 850 emu/cc and 863 K, respectively. See Supplemental Material for the in-plane and out-of-plane hysteresis loops and the *M-T* curve [26].

To study the ultrafast magnetization dynamics of this sample, we use a custom-built TR MOKE magnetometer based on the optical pump-probe technique as shown in Fig. 1(a). Here, the second harmonic ($\lambda = 400$ nm,

repetition rate $= 1$ kHz, pulse width >40 fs) of the amplified femtosecond laser pulse generated from a regenerative amplifier system (Libra, Coherent) is used to excite the dynamics while the fundamental laser pulse ($\lambda = 800$ nm, repetition rate $= 1$ kHz, pulse width approximately 40 fs) is used as a probe to detect the time-resolved polar Kerr signal from the sample. The temporal resolution of the measurement is limited by the cross-correlation between the pump and probe pulses (approximately 120 fs). The probe beam has a diameter of about 100 μm and is normally incident on the sample, whereas the pump beam is kept slightly defocused (the spot size is about 300 μm) and is obliquely (approximately 30° to the normal to the sample plane) incident on the sample maintaining an excellent spatial overlap with the probe spot. A time-resolved Kerr signal is collected from the uniformly excited part of the sample and slight misalignment during the course of the experiment does not significantly affect the pump-probe signal. A large magnetic field of 3.5 kOe is first applied at a small angle of about 10° to the sample plane to saturate its magnetization. This is followed by a reduction of the magnetic field to the bias field value ($H =$ in-plane component of the bias field), which ensures that the magnetization remains saturated along the bias field direction. The tilt of magnetization from the sample plane ensures a finite demagnetizing field along the direction of the pump pulse, which is further modified by the pump pulse to induce precessional dynamics within the sample [17]. In our experiment, a 2-ns time window is used, which gives a damped uniform precession of magnetization. The pump beam is chopped at 373 Hz frequency and the dynamic signal in the probe pulse is detected by using a lock-in amplifier in a phase-sensitive manner. Simultaneous time-resolved reflectivity and Kerr rotation data are measured and no significant breakthrough of one into the other is found. See Supplemental Material for the experimental time-resolved data taken at $H = 2.4$ kOe and $F = 50$ mJ/cm^2 [26]. The probe fluence is kept constant at 2 mJ/cm^2 during the measurement to avoid an additional contribution to the modulation of spin dynamics via laser heating. Pump fluence (F) is varied from 10 to 55 mJ/cm^2 to study the fluence-dependent modulation in magnetization dynamics. All the experiments are performed under ambient conditions and room temperature.

III. RESULTS AND DISCUSSIONS

A. Laser-induced ultrafast demagnetization

When a femtosecond laser pulse interacts with a ferromagnetic thin film in its saturation condition, the magnetization of the system is partially or fully lost within hundreds of femtoseconds as measured by the time-resolved Kerr rotation or ellipticity. This is known as ultrafast demagnetization of the ferromagnet and was first
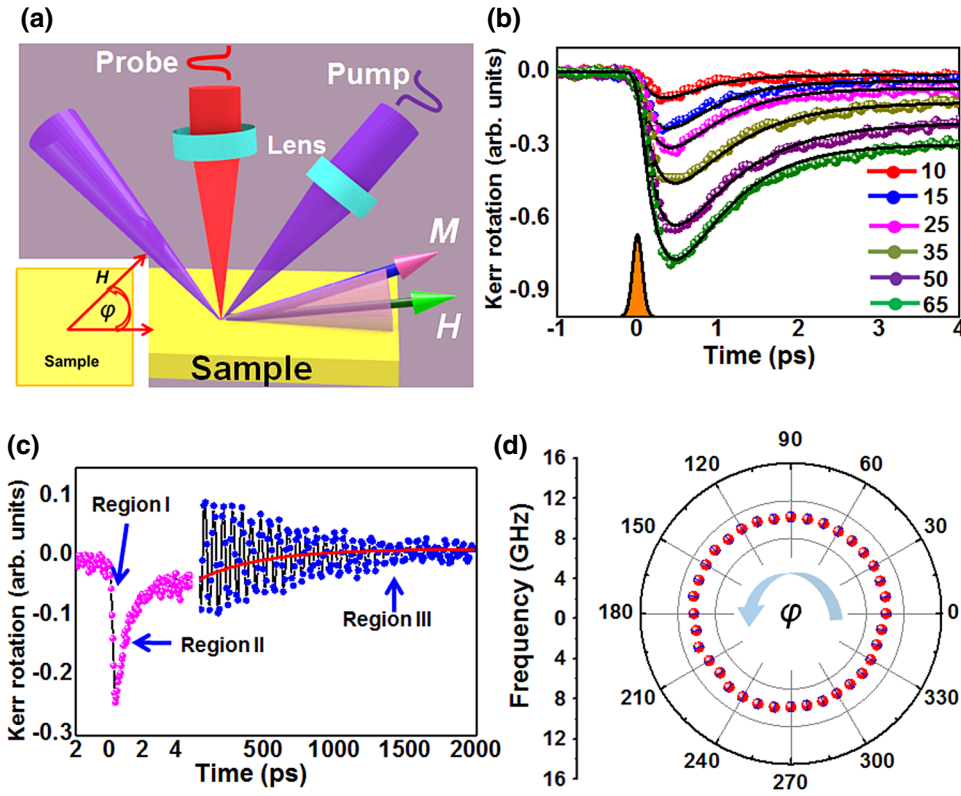
FIG. 1. (a) Schematic of experimental geometry. In the inset, φ is shown as the in-plane rotational angle of H. (b) Pump-fluence dependence of ultrafast demagnetization; solid lines are fitting lines. Pump fluences (F) having units of mJ/cm^2 are mentioned in the numerical figure. The Gaussian envelope of the laser pulse is presented to describe the convolution. (c) Representative time-resolved Kerr rotation data with three distinguished temporal regions for $F = 25$ mJ/cm^2. (d) Angular variation of precessional frequency at $H = 1.1$ kOe for 20-nm-thick Py film. φ is presented in degrees.

observed by Beaurepire *et al.* in 1996 [27]. This is generally followed by a fast recovery of the magnetization within subpicoseconds to a few picoseconds and a slower recovery within tens to hundreds of picoseconds, known as the fast and slow remagnetizations. In many cases, the slower recovery is accompanied by a coherent magnetization precession and damping [17]. In our pump-probe experiment, the sample magnetization is maintained in the saturated state by application of a magnetic field $H = 2.4$ kOe before zero delay. Right after the zero delay and the interaction of the pump pulse with the electrons in the ferromagnetic metal, ultrafast demagnetization takes place. The local magnetization is immediately quenched within the first few hundreds of femtoseconds followed by a subsequent fast remagnetization in next few picoseconds [27]. Figure 1(b) shows the ultrafast demagnetization obtained for different pump fluences. Several models have been proposed over two decades to explain the ultrafast demagnetization [16,28–31]. Out of those, a phenomenological thermodynamic model, called the three-temperature model [27,32,33], has been the most widely used, where the dynamics of these spin fluctuations can be described as

$$\Delta M = \theta(t) \left[-A_1 + \frac{A_2 \tau_{\text{el lat}} - A_1 \tau_{\text{el sp}}}{\tau_{\text{el lat}} - \tau_{\text{el sp}}} e^{-(t/\tau_{\text{el sp}})} \right.$$
$$\left. + \frac{A_1 - A_2}{\tau_{\text{el lat}} - \tau_{\text{el sp}}} \tau_{\text{el lat}} e^{-(t/\tau_{\text{el lat}})} \right] M_0 \otimes \Gamma(t). \quad (1)$$

This is an approximated form based on the assumption that the electron temperature rises instantaneously upon laser excitation and can be applied to fit time-resolved Kerr rotation data taken within a few picoseconds timescale. The whole system is divided into three subsystems: electron, spin, and lattice systems. On laser excitation, the hot electrons are created above the Fermi level. Then during energy rebalancing between the subsystems, quenched magnetization relaxes back to the initial state. The two exponential functions in the above equation mirror the demagnetization given by the demagnetization time ($\tau_{\text{el sp}}$) for energy transfer between electron spin and the decay of electron temperature ($\tau_{\text{el lat}}$) owing to the transfer of energy to the lattice. In addition to these characteristic time constants, the spin-lattice relaxation time can also be extracted by including another exponential term in the above equation if the spin specific heat is taken into account [34]. θ is the Heaviside step function and $\Gamma(t)$ stands for the Gaussian function to be convoluted with the laser-pulse envelope for determining the temporal resolution (showing the cross-correlation between the probe and pump pulse). The constant, A_1, indicates the ratio between the amount of magnetization after equilibrium between electrons, spins, and lattice is restored and the initial magnetization. A_2 is proportional to the initial electronic temperature rise. We have plotted A_1 and A_2, normalized with their values at the highest fluence, as a function of pump fluence in Fig. 3S of the Supplemental Material, which shows that the magnitude of both

parameters increases with laser fluence [26]. We observe that with increasing fluence, the demagnetization time is negligibly varied within a range of 250 ± 40 fs. The weak or no correlation between the pump fluence and the demagnetization rate describes the intrinsic nature of the spin scattering, governed by various mechanisms including the Elliott-Yafet mechanism [35]. Another important observation here is that the delay of the demagnetization processes, which is the time delay between the pump pulse (FWHM $\approx 130 \pm 20$ fs) and the starting point of the ultrafast demagnetization, becomes shorter due to the increase in pump fluences. A plausible explanation for this is the dependence of the delay of demagnetization on the electron-thermalization time, which is eventually proportional to electron density or pump fluences [36]. On the other hand, fast remagnetization time is found to increase noticeably from 0.40 ± 0.05 ps to 0.80 ± 0.05 ps within the experimental fluence range of $10 - 55$ mJ/cm^2. The larger the pump fluence is, the higher is the electron temperature and also the spin temperature. Therefore, it is reasonable that the magnetization recovery time increases with the pump fluence.

B. Pump-fluence-dependent modulation in Gilbert damping

Figure 1(c) shows the representative Kerr rotation data for $F = 25$ mJ/cm^2 consisting of three temporal regions, i.e., ultrafast demagnetization, fast remagnetization, and slow remagnetization superposed with damped precession within the time window of 2 ns. We process the magnetization precession part after subtracting a bi-exponential background to estimate the damping and its modulation. The slower remagnetization is mainly due to heat diffusion from the lattice to the substrate and the surroundings. Within our experimental fluence range, the slow remagnetization time increases from approximately 0.4 ns to approximately 1.0 ns. The precessional dynamics is described by the phenomenological LLG equation,

$$\frac{d\vec{M}}{dt} = -\gamma \ \vec{M} \times \vec{H}_{\text{eff}} + \frac{\alpha}{M_s}\vec{M} \times \frac{d\vec{M}}{dt}, \qquad (2)$$

where γ is the gyromagnetic ratio, M is magnetization, α the is Gilbert damping constant, and H_{eff} is the effective magnetic field consisting of several field components. The variation of precessional frequency with the angle between the sample plane and the bias magnetic field direction is plotted in Fig. 1(d), which reveals that there is no uniaxial anisotropy present in this sample.

The energy deposited by the pump pulse, in terms of heat within the probed volume, plays a very crucial role in modification of local magnetic properties, i.e., magnetic moment, anisotropy, coercivity, magnetic susceptibility, etc. With increasing fluence, the precessional frequency experiences a redshift [20,25]. Thus, at the onset of the

precessional dynamics (about 10 ps from zero delay), for a relatively high fluence, the initial frequency (f_i) will be smaller than its intrinsic value (in the absence of any significant heat dissipation). As time progresses and the sample magnetization gradually attains its equilibrium value, the precessional frequency continuously changes, causing a temporal chirping of the damped oscillatory Kerr signal. The frequency shift can be estimated from the amount of temporal chirping [37]. Figure 2(a) shows the background-subtracted time-resolved Kerr rotation data (precessional part) for different pump fluences fitted with a damped sinusoidal function with added temporal chirping,

$$\theta_k \ = Ae^{-t/\tau} \ \sin[2\pi(f_i + bt)t + \Phi],$$

where A, τ, f_i, b, and Φ are the amplitude of the magnetization precession, the relaxation time, the initial precessional frequency, the chirp parameter, and the initial phase, respectively. At this point, we are unsure of the exact nature of the damping, i.e., it may consist of both intrinsic and extrinsic mechanisms and hence we term it as the effective damping parameter (α_{eff}) which can be extracted using the following formula [38]:

$$\alpha_{\text{eff}} = \frac{1}{\gamma \tau[H + (4\pi M_{\text{eff}}/2)]}, \qquad (3)$$

where $\gamma = 1.83 \times 10^7$ Hz/Oe for Py and M_{eff} is the effective magnetization including pump-induced changes at $H = 2.4$ kOe. This formula is exploited to extract a precise effective damping parameter in the moderate bias-field regime. The variation of relaxation time and effective damping are plotted with pump fluence in Figs. 2(b) and 2(c). Here, τ decreases with fluence while damping increases significantly with respect to its intrinsic value within this fluence range. We repeat the experiment for two different field values (2.4 and 1.8 kOe). The slope of fluence-dependent damping remains unaltered for both the field values. We also observe an increase in the relative amplitudes of precession with pump fluence as shown in the inset of Fig. 2(c). To verify the transient nature of the damping, we perform another set of experiments where the probed area is exposed to different pump fluences (F_i) for several minutes. After the irradiation, the precessional dynamics is measured from that area with fixed probe and pump fluences of 2 and 10 mJ/cm^2, respectively. We find that damping remains almost constant for all the measurements [as shown in Fig. 2(d)]. These results demonstrate that the enhancement of damping is transient and only exists in the presence of a high pump fluence, but drops to its original value when the pump laser is set to the initial fluence.

The bias-field dependence of precessional dynamics at four different pump fluences is studied to gain more insight into the origin of the fluence-dependent damping. First,
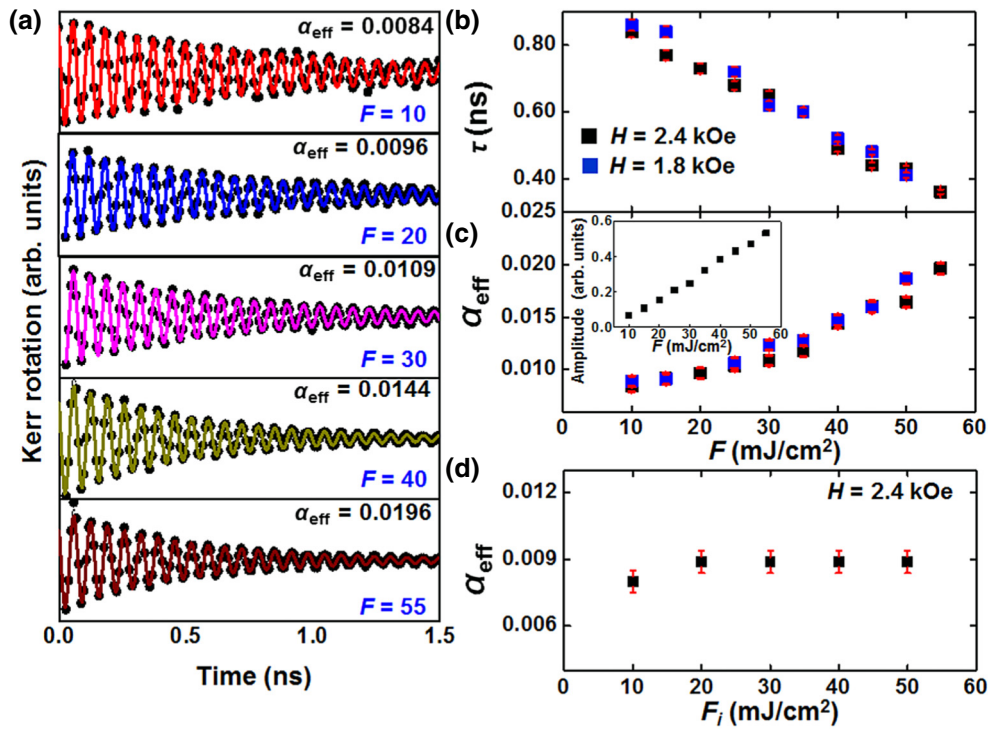
FIG. 2. (a) Background-subtracted time-resolved Kerr rotation data for different pump fluences at $H = 2.4$ kOe. F has units of mJ/cm^2 and is noted in the numerical figure. Solid lines are fitting lines. Pump-fluence dependence of (b) relaxation time (τ) and (c) effective damping (α_{eff}). Black and blue symbols represent the variation of these parameters at two different field values, $H = 2.4$ and 1.8 kOe, respectively. The amplitude of the precession is also plotted with pump fluence for $H = 2.4$ kOe. (d) Variation of effective damping with irradiation fluence (F_i) at $H = 2.4$ kOe. In order to check the possible damage in the sample due to high-fluence values, the pump fluence is taken up to the targeted value of F_i for several minutes followed by a reduction of the pump fluence to a constant value of 10 mJ/cm^2 and the pump-probe measurement is performed. The damping coefficient is found to be unaffected by the irradiation fluence as shown in (d).

we plot the average frequency (f_{FFT}) with the bias field which is obtained from the FFT of the precessional data in Fig. 3(a). The experimental data points are fitted with the Kittel formula

$$f_{FFT} = \frac{\gamma}{2\pi}\sqrt{H(H + 4\pi M_{eff})}. \qquad (4)$$

M_{eff} is the effective magnetization of the sample. Figure 3(b) shows that the effective magnetization does not vary much within the applied fluence range. Thus, we infer that with increasing fluence, there is no induced anisotropy developing in the system that can modify the effective damping up to this extent [23]. The variations of relaxation time with the bias field for four different pump fluences are plotted in Fig. 3(c). Relaxation time is increased with decreasing field for each case, but for the higher fluence regime, these values seem to be fluctuating. This dependence of τ on the field was fitted with Eq. (3) to extract the damping coefficient at different fluence values. We have further plotted the damping coefficient as a function of precession frequency (f_{FFT}) [see Fig. 4S of the Supplemental Material], which shows an invariance of α_{eff} with f_{FFT} [26].

From that, we can infer that the damping coefficient in our sample within the experimental field and fluence regime are intrinsic in nature and hence, we may now term it as the intrinsic damping coefficient α_0 [39,40]. The extrinsic contributions to damping mainly come from the magnetic anisotropy field, two-magnon scattering, multimodal dephasing for excitation of several spin-wave modes, etc., which are negligible in our present case.

Figure 3(d) shows the variation of α_0 with pump fluence, which shows that even the intrinsic damping is significantly increasing with pump fluence [20,41]. For the generation of perpendicular standing spin-wave modes, the film needs to be thick enough. Though the film thickness is 20 nm here, within the applied bias-field range, we have not found any other magnetic mode appearing with the uniform Kittel mode within the frequency window we have used. See Supplemental Material for further discussion [26]. Also, for 20-nm-thick Py film, the effect of an eddy current will be negligible [42]. The overlap between the spatial profile of the focused probe and the pump-laser spot may lead to the generation of magnons that propagate away from the region that is being probed. Generally,
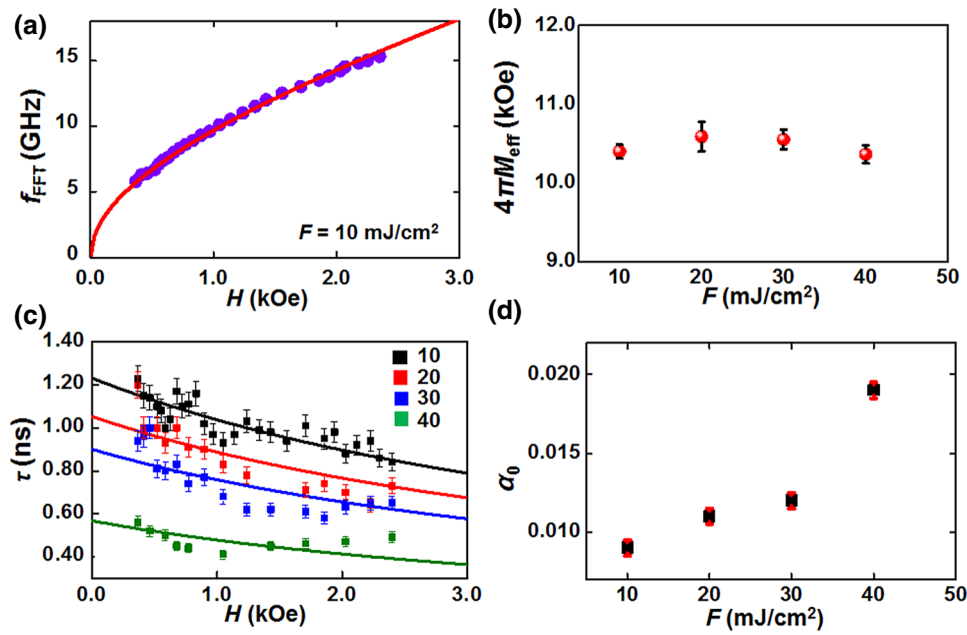
FIG. 3. (a) Bias field dependence of precessional frequency for $F = 10$ mJ/cm^2. The red solid line indicates the Kittel fit. (b) Pump-fluence dependence of effective magnetization (M_{eff}) of the probed volume. (c) Bias-field dependence of relaxation time (τ) for four different fluences. F has units of mJ/cm^2 and is mentioned in the numerical figures. Solid lines are the fitted data. (d) Variation of intrinsic Gilbert damping (α_0) with pump fluence.

enhancement of nonlocal damping by spin-wave emission becomes significant when the excitation area is less than 1 μm. Recently, J. Wu *et al.* showed that propagation of magnetostatic spin waves could be significant even for probed regions tens of microns in size [43]. Also, by generating a spin-wave trap in the pump-probe experiment, modification of the precessional frequency in a ferromagnetic thin film due to accumulation and dissipation of thermal energy within the probed volume has been reported [44]. During our experiment, the overlap between the probe and pump spot is carefully maintained and the Kerr signal is collected from the uniformly excited part of the sample so that a slight misalignment during the course of the experiment does not introduce any nonlocal effects. We will now substantiate our results with some theoretical arguments, which involve the calculation of electronic temperature rise in the system due to the application of a higher pump fluence. The electronic temperature (T_e) is related to the absorbed laser energy per unit volume (E_a) according to the following equation [45]:

$$E_a = \xi(T_e^2 - T_0^2)/2, \tag{5}$$

where ξ is the electronic specific heat of the system and T_0 is the initial electronic temperature (room temperature here). First, we estimate E_a according to the optical parameters of the sample by using the following equation:

$$E_a = [(1 - e^{-(d/\psi)})F(1 - R)/d], \tag{6}$$

where d is the sample thickness, ψ is the optical penetration depth (approximately 17 nm for a 400-nm pump laser in a 20-nm-thick Py film), R is the reflectivity of the sample (0.5 measured for the Py film), and F is the

applied pump fluence. By solving Eqs. (5) and (6), we observe that T_e increases from approximately 1800 to 4500 K within our experimental fluence range of 10 to 55 mJ/cm^2. See Supplemental Material for extraction of decay time of the electron temperature and other relevant parameters (i.e., E_a, T_e at various fluences) [26,45–48]. The sample remains in its magnetized state even if the electronic temperature exceeds the Curie temperature T_c. Importantly, the ratio of the system temperature, T (as the decay of the electronic temperature is strongly correlated with the rise of the lattice temperature) to T_c is affecting the magnetization relaxation time, which fundamentally depends on susceptibility. Accordingly, damping should be proportional to susceptibility, which is strongly temperature dependent [42]. Various procedures for exciting precessional dynamics in ferromagnets show the different mechanisms responsible for the exploration of different energy-dissipation channels. The spin-phonon interaction mechanism, which historically has been thought to be the main contribution to magnetization damping, is important for picosecond-nanosecond applications at high temperatures such as spin caloritronics. But for laser-induced magnetization dynamics, where spin-flips occur mainly due to electron scattering, the quantum Landau-Lifshitz-Bloch equation is sometimes exploited to explain the temperature dependence of damping by considering a simple spin-electron interaction as a source for magnetic relaxation [49]. This approach suggests that increasing the ratio between the system temperature and Curie temperature induces electron-impurity led spin-dependent scattering. Even slightly below T_c, a pure change in the magnetization magnitude occurs, which causes the enhancement of damping. Our experimental results also reveal that the precession amplitude and damping are subjected to a sudden

change for $F > 30$ mJ/cm^2. The energy density deposited in the probed volume is proportional to the pump fluence. For a higher fluence, the temperature dependence of the electronic specific heat plays a major role. The increase in the electronic specific heat value with temperature may lead to a longer thermal-relaxation time. We infer that the relative balance between the energy deposited into the lattice and the electron system is also different for a higher fluence regime compared to that in the lower fluence regime. Thus, the system temperature remains well above the Curie temperature for $F > 30$ mJ/cm^2 during the onset of precession for $t \geq 10$ ps. This may open up an additional energy-dissipation channel for the magnetization relaxation process over nanoseconds timescale. Sometimes, within a very short timescale, the spin temperature can go beyond the Curie temperature, leading toward the formation of a paramagnetic state, but that is a highly nonequilibrium case [50]. However, we believe that in our experiment, even for the high fluence limit and in local thermal equilibrium, the ferromagnetic to paramagnetic transition is not observed. Repetitive measurements establish the reversibility of the damping parameter and the bias-magnetic-field dependence of the precessional frequency confirms the ferromagnetic nature of the sample.

C. Frequency modulation and temporal chirping

Pump fluence also eventually modulates the precessional frequency by introducing temporal chirping into the uniform precession. After immediate arrival of the pump pulse, because of an enhancement of the surface temperature, the net magnetization is reduced in a picosecond timescale, which results in chirping of the precessional oscillation. The initial frequency (f_i) is reduced with respect to its intrinsic value at a constant field. But when the probed volume cools with time, the spins try to retain their original precessional frequency. Thus, within a fixed time window, the average frequency (f_{FFT}) also undergoes a slight modification. In the high fluence regime, a significant redshift occurs in both f_{FFT} and f_i. For $H = 2.4$ and 1.8 kOe, modulation of the frequency is found to be 0.020 GHz.cm^2/mJ for f_{FFT} and 0.028 GHz.cm^2/mJ for f_i from the slope of the linear fit [as shown in Fig. 4(a)]. The f_{FFT} is reduced by 7.2% of the extrapolated value at zero pump fluence for both the fields.

On the other hand, f_i is decreased by 8.7% of its zero pump value for the highest pump fluence. The temporal chirp parameter, b shows a very large enhancement within the experimental fluence range [Fig. 4(b)]. For $H = 2.4$ kOe, b increases up to ten times (from 0.03 GHz/ns to 0.33 GHz/ns) in this fluence limit, which implies an increase in the frequency of 0.66 GHz. Within our experimental scan window (2 ns), the maximum frequency shift is found to be 4.5% for $F = 55$ mJ/cm^2. For another bias field ($H = 1.8$ kOe), the enhancement of the chirp parameter follows a similar trend. This ultrafast modulation is attributed to the thermal effect on the
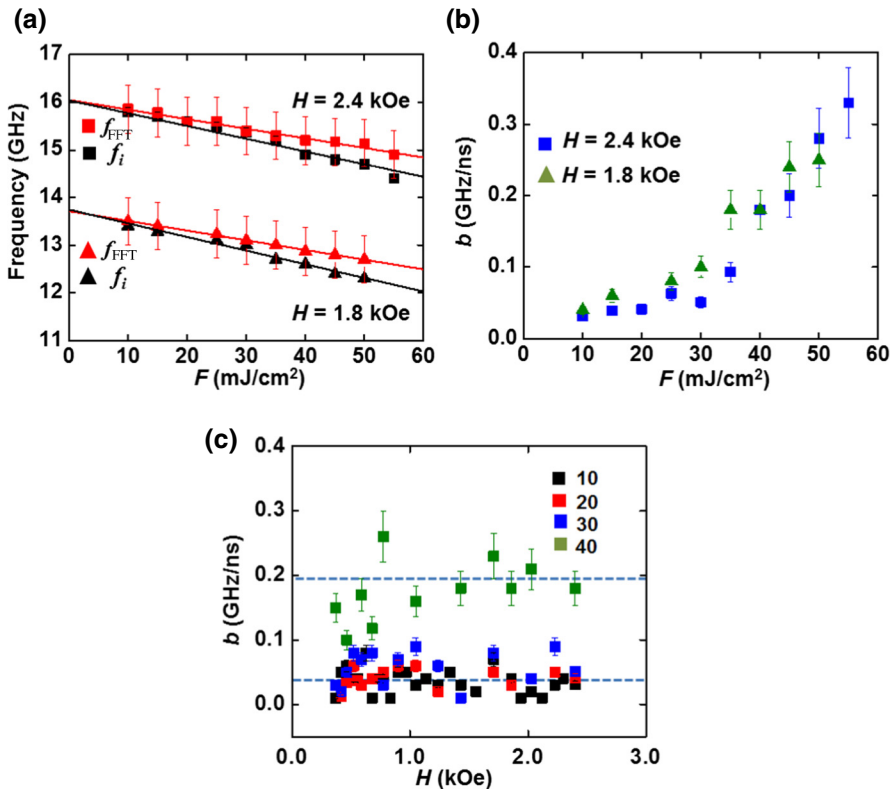

FIG. 4. (a) Pump-fluence dependence of precessional frequencies for $H = 2.4$ and 1.8 kOe. Red and black symbols represent the variations of average frequency (f_{FFT}) and initial frequency (f_i), respectively. (b) Variation of temporal chirp parameter "b" with pump fluence for two different magnetic field values. (c) Variation of temporal chirp parameter with bias field for four different pump fluences. F has units of mJ/cm^2 and is mentioned in the numerical figure. Dotted lines are used as a guide to the eye.

local magnetic properties within the probed volume and is inferred to be reversible [37]. We also plot the variation of b with applied bias field for four different pump fluences. It seems to be almost constant for all the field values in a moderate fluence regime [as shown in Fig. 4(c)]. But for $F = 40$ mJ/cm^2, the data points are relatively scattered and large errors are considered to explain those fluctuations.

IV. CONCLUSION

In essence, a fluence-dependent study of ultrafast magnetization dynamics in Py thin film reveals a very weak correlation between ultrafast demagnetization time and Gilbert damping within our experimental fluence range. We report a large enhancement of damping with pump fluence. From the bias field as well as the pump-fluence dependence of experimentally obtained dynamical parameters, we have excluded all the possible extrinsic contributions and observe a pump-induced modulation of intrinsic Gilbert damping. Also, from repetitive measurements with different pump irradiations, we show that the pump-induced changes are reversible in nature. Enhancement of the system temperature to Curie temperature ratio is believed to be responsible for the increment in remagnetization times and damping. The temporal chirp parameter has been found to be increased by up to ten times within the experimental fluence range, while the frequency experiences a significant redshift. From an application point of view, the increasing demand for faster and more efficient magnetic memory devices has led the scientific community in the extensive research field of ultrafast magnetization dynamics. Our results will further enlighten the understanding of the modulation of magnetization dynamics in ferromagnetic systems in the presence of higher pump fluences. Low damping materials are preferred because it is easier to switch their magnetization in expense of smaller energy, lower write current in spin transfer torque magnetic random-access memories devices and longer propagation length of spin waves in magnonic devices. On the other hand, higher damping is also required to stop the post-switching ringing of the signal. The results also have important implications in the emergent field of all-optical helicity-dependent switching [51–53]. In this context, the transient modulation of Gilbert damping and other dynamical parameters in ferromagnetic materials are of fundamental interest for characterizing and controlling ultrafast responses in magnetic structures.

[1] O. Hellwig, A. Berger, T. Thomson, E. Dobisz, Z. Z. Bandic, H. Yang, D. S. Kercher, and E. E. Fullerton, Separating dipolar broadening from the intrinsic switching field distribution in perpendicular patterned media, Appl. Phys. Lett. **90**, 162516 (2007).

[2] S. Tehrani, E. Chen, M. Durlam, M. DeHerrera, J. M. Slaughter, J. Shi, and G. Kerszykowski, High density submicron magnetoresistive random access memory, J. Appl. Phys. **85**, 5822 (1999).

[3] L. Landau and E. Lifshits, On the theory of the dispersion of magnetic permeability in ferromagnetic bodies, Phys. Zeitsch. der Sow. **8**, 153 (1935).

[4] T. L. Gilbert, A phenomenological theory of damping in ferromagnetic materials, IEEE Trans. Magn. **40**, 6 (2004).

[5] P. He, X. Ma, J. W. Zhang, H. B. Zhao, G. Lupke, Z. Shi, and S. M. Zhou, Quadratic Scaling of Intrinsic Gilbert Damping with Spin-Orbital Coupling in L10 FePdPt Films: Experiments and ab initio Calculations, Phys. Rev. Lett. **110**, 077203 (2013).

[6] B. Heinrich, J. F. Cochran, and K. Myrtle, The exchange splitting of phonon assisted microwave transmission at 9.5 GHz, J. Appl. Phys. **53**, 2092 (1982).

[7] P. Krivosik, N. Mo, S. Kalarickal, and C. E. Patton, Hamiltonian formalism for two magnon scattering microwave relaxation: Theory and applications, J. Appl. Phys. **101**, 083901 (2007).

[8] J. O. Rantschler, R. D. McMichael, A. Castillo, A. J. Shapiro, W. F. Egelhoff, B. B. Maranville, D. Pulugurtha, A. P. Chen, and L. M. Connors, Effect of 3d, 4d, and 5d transition metal doping on damping in permalloy thin films, J. Appl. Phys. **101**, 033911 (2007).

[9] Y. Tserkovnyak, A. Brataas, and G. E. W. Bauer, Spin pumping and magnetization dynamics in metallic multilayers, Phys. Rev. B **66**, 224403 (2002).

[10] A. Ganguly, R. M. Rowan-Robinson, A. Haldar, S. Jaiswal, J. Sinha, A. T. Hindmarch, D. A. Atkinson, and A. Barman, Time-domain detection of current controlled magnetization damping in Pt/Ni81Fe19 bilayer and determination of Pt spin Hall angle, Appl. Phys. Lett. **105**, 112409 (2014).

[11] K. Lenz, H. Wende, W. Kuch, K. Baberschke, K. Nagy, and A. Jánossy, Two-magnon scattering and viscous Gilbert damping in ultrathin ferromagnets, Phys. Rev. B **73**, 144424 (2006).

[12] Y. Zhao, Q. Song, S. H. Yang, T. Su, W. Yuan, S. S. P. Parkin, J. Shi, and W. Han, Experimental investigation of temperature-dependent Gilbert damping in permalloy thin films, Sci. Rep. **6**, 22890 (2016).

[13] V. Kamberský, FMR linewidth and disorder in metals, Czech J. Phys. B **34**, 1111 (1984).

[14] J. M. Beaujour, D. Ravelosona, I. Tudosa, E. E. Fullerton, and A. D. Kent, Ferromagnetic resonance linewidth in ultrathin films with perpendicular magnetic anisotropy, Phys. Rev. B **80**, 180415R (2009).

[15] M. R. Freeman, R. R. Ruf, and R. J. Gambino, Picosecond pulsed magnetic fields for studies of ultrafast magnetic phenomena, IEEE Trans. Magn. **27,** 4840 (1991).

[16] G. P. Zhang and W. Hübner, Laser-Induced Ultrafast Demagnetization in Ferromagnetic Metals, Phys. Rev. Lett. **85,** 3025 (2000).

[17] M. van Kampen, C. Jozsa, J. T. Kohlhepp, P. LeClair, L. Lagae, W. J. M. de Jonge, and B. Koopmans, All-Optical Probe of Coherent Spin Waves, Phys. Rev. Lett. **88,** 227201 (2002).

[18] A. Barman, S. Wang, J. D. Maas, A. R. Hawkins, S. Kwon, A. Liddle, J. Bokor, and H. Schmidt, Magneto-optical observation of picosecond dynamics of single nanomagnets, Nano Lett. **6,** 2939 (2006).

[19] A. Barman and J. Sinha, *Spin dynamics and damping in ferromagnetic thin films and nanostructures* (Springer, Switzerland, 2018).

[20] G. M. Muller, M. Munzenberg, G.-X. Miao, and A. Gupta, Activation of additional energy dissipation processes in the magnetization dynamics of epitaxial chromium dioxide films, Phys. Rev. B **77,** 020412(R) (2008).

[21] S. Y. An, P. Krivosik, M. A. Kraemer, H. M. Olson, A. V. Nazarov, and C. E. Patton, High power ferromagnetic resonance and spin wave instability processes in permalloy thin films, J. Appl. Phys. **96,** 1572 (2004).

[22] W. Peng, Y. T. Hsia, K. Sendur, and T. McDaniel, Thermomagneto-mechanical analysis of head–disk interfacevin heat assisted magnetic recording, Tribol. Int. **38,** 588 (2005).

[23] B. Liu, X. Ruan, Z. Wu, H. Tu, J. Du, J. Wu, X. Lu, L. He, R. Zhang, and Y. Xu, Transient enhancement of magnetization damping in CoFeB film via pulsed laser excitation, Appl. Phys. Lett. **109,** 042401 (2016).

[24] Z. Chen, M. Yi, M. Chen, S. Li, S. Zhou, and T. Lai, Spin waves and small intrinsic damping in an in-plane magnetized FePt film, Appl. Phys. Lett. **101,** 222402 (2012).

[25] S. Mizukami, H. Abe, D. Watanabe, M. Oogane, Y. Ando, and T. Miyazaki, Gilbert damping for various $Ni_{80}Fe_{20}$ thin films investigated using all-optical pump–probe detection and ferromagnetic resonance, Appl. Phys. Exp. **1,** 121301 (2008).

[26] See Supplemental Material at http://link.aps.org/supplemental/10.1103/PhysRevApplied.10.054037, which includes detailed discussion on sample characterization, time resolved reflectivity and Kerr rotation measurement, variation of A_1 and A_2 with pump fluence, variation of effective damping with frequency, uniform precessional mode and evolution of electronic temperature.

[27] E. Beaurepaire, J. C. Merle, A. Daunois, and J. Y. Bigot, Ultrafast Spin Dynamics in Ferromagnetic Nickel, Phys. Rev. Lett. **76,** 4250 (1996).

[28] S. I. Anisimov, B. L. Kapeliovich, and T. L. Perelman, Electron emission from metal surfaces exposed to ultrashort laser pulses, Sov. Phys. JETP **39**, 2 (1974).

[29] M. Krauß, T. Roth, S. Alebrand, D. Steil, M. Cinchetti, M. Aeschlimann, and H. C. Schneider, Ultrafast demagnetization of ferromagnetic transition metals: The role of the Coulomb interaction, Phys. Rev. B **80,** 180407 (2009).

[30] G. Malinowski, F. Dalla Longa, J. H. H. Rietjens, P. V. Paluskar, R. Huijink, H. J. M. Swagten, and B. Koopmans, Control of speed and efficiency of ultrafast demagnetization by direct transfer of spin angular momentum, Nat. Phys. **4,** 855 (2008).

[31] D. Rudolf, C. La-O-Vorakiat, M. Battiato, R. Adam, J. M. Shaw, E. Turgut, P. Maldonado, S. Mathias, P. Grychtol, H. T. Nembach, T. J. Silva, M. Aeschlimann, H. C. Kapteyn, M. M. Murnane, C. M. Schneider, and P. M. Oppeneer, Ultrafast magnetization enhancement in metallic multilayers driven by superdiffusive spin current, Nat. Comm. **3,** 1037 (2012).

[32] F. Dalla Longa, J. T. Kohlhepp, W. J. M. de Jonge, and B. Koopmans, Influence of photon angular momentum on ultrafast demagnetization in nickel, Phys. Rev. B **75,** 224431 (2007).

[33] J. Walowski, G. Muller, M. Djordjevic, M. Munzenberg, M. Klaui, A. F. Vaz, and J. A. C. Bland, Energy Equilibration Processes of Electrons, Magnons, and Phonons at the Femtosecond Time Scale, Phys. Rev. Lett. **101,** 237401 (2008).

[34] U. Atxitia, O. Chubykalo-Fesenko, J. Walowski, A. Mann, and M. Münzenberg, Evidence for thermal mechanisms in laser-induced femtosecond spin dynamics, Phys. Rev. B **81,** 174401 (2010).

[35] B. Koopmans, J. J. M. Ruigrok, F. Dalla Longa, and W. J. M. de Jonge, Unifying Ultrafast Magnetization Dynamics, Phys. Rev. Lett. **95,** 267207 (2005).

[36] X. Liu, Z. Xu, R. Gao, H. Hu, Z. Chen, Z. Wang, J. Du, S. Zhou, and T. Lai, Dynamics of magnetization, reversal, and ultrafast demagnetization of TbFeCo amorphous films, Appl. Phys. Lett. **92,** 232501 (2008).

[37] Y. Liu, L. R. Shelford, V. V. Kruglyak, R. J. Hicken, Y. Sakuraba, M. Oogane, and Y. Ando, Optically induced magnetization dynamics and variation of damping parameter in epitaxial Co_2MnSi Heusler alloy films, Phys. Rev. B **81,** 094402 (2010).

[38] J. Walowski, M. Djordjevic Kaufmann, B. Lenk, C. Hamann, J. McCord, and M. Munzenberg, Intrinsic and non-local Gilbert damping in polycrystalline nickel studied by Ti : Sapphire laser fs spectroscopy, J. Phys. D: Appl. Phys. **41,** 164016 (2008).

[39] G. Woltersdorf, M. Buess, B. Heinrich, and C. H. Back, Time Resolved Magnetization Dynamics of Ultrathin Fe(001) Films: Spin-Pumping and Two-Magnon Scattering, Phys. Rev. Lett. **95,** 037401 (2005).

[40] J. A. King, A. Ganguly, D. M. Burn, S. Pal, E. A. Sallabank, T. P. A. Hase, A. T. Hindmarch, A. Barman, and D. Atkinson, Local control of magnetic damping in ferromagnetic/non-magnetic bilayers by interfacial intermixing induced by focused ion-beam irradiation, Appl. Phys. Lett. **104,** 242410 (2014).

[41] A. Capua, S. H. Yang, T. Phung, and S. S. P. Parkin, Determination of intrinsic damping of perpendicularly magnetized ultrathin films from time-resolved precessional magnetization measurements, Phys. Rev. B **92,** 224402 (2015).

[42] B. Heinrich and J. A. C. Bland, Spin relaxation in magnetic metallic layers and multilayers, in *Ultrathin magnetic structures: fundamentals of nanomagnetism*, edited by Bland J. A. C. (Springer, New York, 2005), Vol. 3.

[43] J. Wu, N. D. Hughes, J. R. Moore, and R. J. Hicken, Excitation and damping of spin excitations in ferromagnetic thin films, J. Magn. Magn. Mater. **241,** 96 (2002).

[44] F. Busse, M. Mansurova, B. Lenk, M. von der Ehe, and M. Münzenberg, A scenario for magnonic spin-wave traps, Sci. Rep. **5,** 12824 (2015).

[45] E. Carpene, E. Mancini, C. Dallera, M. Brenna, E. Puppin, and S. De Silvestri, Dynamics of electron-magnon interaction and ultrafast demagnetization in thin iron films, Phys. Rev. B **78,** 174422 (2008).

[46] J. Mendil, P. Nieves, O. Chubykalo-Fesenko, J. Walowski, T. Santos, S. Pisana, and M. Munzenberg, Resolving the role of femtosecond heated electrons in ultrafast spin dynamics, Sci. Rep. **4,** 3980 (2014).

[47] R. W. Schoenlein, W. Z. Lin, J. G. Fujimoto, and G. L. Eesley, Femtosecond Studies of Nonequilibrium Electronic Processes in Metals, Phys. Rev. Lett. **58,** 1680 (1987).

[48] Z. Lin, Leonid V. Zhigilei, and V. Celli, Electron-phonon coupling and electron heat capacity of metals under conditions of strong electron-phonon nonequilibrium, Phys. Rev. B **77,** 075133 (2008).

[49] P. Nieves, D. Serantes, U. Atxitia, and O. Chubykalo-Fesenko, Quantum Landau-Lifshitz-Bloch equation and its comparison with the classical case, Phys. Rev. B **90,** 104428 (2014).

[50] N. Kazantseva, U. Nowak, R. W. Chantrell, J. Hohlfeld, and A. Rebei, Slow recovery of the magnetisation after a sub-picosecond heat pulse, EPL **81,** 27004 (2008).

[51] G. M. Choi, A. Schleife, and D. G. Cahill, Optical-helicity-driven magnetization dynamics in metallic ferromagnets, Nat. Comm. **8,** 15085 (2017).

[52] T. D. Cornelissen, R. Córdoba, and B. Koopmans, Microscopic model for all optical switching in ferromagnets, Appl. Phys. Lett. **108,** 142405 (2016).

[53] Md. S El Hadri, M. Hehn, G. Malinowski, and S. Mangin, Materials and devices for all-optical helicity dependent switching, J. Phys. D: Appl. Phys. **50,** 133002 (2017).